Cheng, Qiang; Ahmad, Zeeshan; Kaario, Ossi; Vuorinen, Ville; Larmi, Martti

Experimental study on tri-fuel combustion using premixed methane-hydrogen mixtures ignited by a diesel pilot

Published in:
International Journal of Hydrogen Energy

DOI:
10.1016/j.ijhydene.2021.03.215

Published: 11/06/2021

Document Version
Publisher's PDF, also known as Version of record

Please cite the original version:
Cheng, Q., Ahmad, Z., Kaario, O., Vuorinen, V., & Larmi, M. (2021). Experimental study on tri-fuel combustion using premixed methane-hydrogen mixtures ignited by a diesel pilot. *International Journal of Hydrogen Energy*, *46*(40), 21182-21197. https://doi.org/10.1016/j.ijhydene.2021.03.215

INTERNATIONAL JOURNAL OF HYDROGEN ENERGY 46 (2021) 21182–21197

Available online at www.sciencedirect.com

ScienceDirect

journal homepage: www.elsevier.com/locate/he

Experimental study on tri-fuel combustion using premixed methane-hydrogen mixtures ignited by a diesel pilot

*Qiang Cheng**, *Zeshan Ahmad, Ossi Kaario, Ville Vuorinen, Martti Larmi*

Department of Mechanical Engineering, Aalto University, 02150-Espoo, Finland

HIGHLIGHTS

- A comprehensive study on diesel pilot tri-fuel combustion has been conducted in a compression ignition engine.
- The H_2 concentration and charge-air temperature were parametrically applied to study their effects on engine performance.
- A short-time Fourier transfer method was employed to estimate the combustion stability.
- A continuous wavelet transfer method was adopted to assess the cycle-to-cycle variations.

ARTICLE INFO

Article history:
Received 15 December 2020
Received in revised form
23 March 2021
Accepted 25 March 2021
Available online 23 April 2021

Keywords:
Tri-fuel
Ignition behavior
Combustion stability
CCV
Engine performance

ABSTRACT

A comprehensive investigation on diesel pilot spray ignited methane-hydrogen (CH_4–H_2) combustion, tri-fuel combustion (TF), is performed in a single-cylinder compression ignition (CI) engine. The experiments provide a detailed analysis of the effect of H_2 concentration (based on mole fraction, M_{H2}) and charge-air temperature (T_{air}) on the ignition behavior, combustion stability, cycle-to-cycle (CCV) and engine performance. The results indicate that adding H_2 from 0 to 60% shortens the ignition delay time (IDT) and combustion duration (based on CA90) up to 33% and 45%, respectively. Thereby, H_2 helps to increase the indicated thermal efficiency (ITE) by as much as 10%. Furthermore, to gain an insight into the combustion stability and CCV, the short-time Fourier transform (STFT) and continuous wavelet transform (CWT) methodologies are applied to estimate the combustion stability and CCV of the TF combustion process. The results reveal that the pressure oscillation can be reduced up to 4 dB/Hz and the CCV by 50% when $M_{H2} < 60\%$ and $T_{air} < 55\,^{\circ}C$. However, when $M_{H2} > 60\%$ and $T_{air} > 40\,^{\circ}C$, abnormal combustion and knocking are observed.

Introduction

To meet the climate and air quality goals, the governments are signaling to the world to move to zero-emission vehicles. The conventional internal combustion engines (ICEs) are facing a huge challenge from electrification due to their emission issues. Many countries and a dozen cities or states have announced the phase-out of fossil fuel-driven vehicles by 2040

* *Corresponding author.*
E-mail address: qiang.cheng@aalto.fi (Q. Cheng).

https://doi.org/10.1016/j.ijhydene.2021.03.215

Nomenclature

AC	Aromatic content
ATDC	After top dead center
aHRR	Apparent heat release rate
CAD	Crank angle degree
CCV	Cycle-to-Cycle variations
CHR	Cumulative heat release
CH_4	Methane
CI	Compression ignition
CN	Cetane number
COV	Coefficient of variation
CWT	Continuous wavelet transform
DF	Dual fuel
EHVA	Electrohydraulic valve actuator
IDT	Ignition delay timing
IMEP	Indicated mean efficient pressure
ITE	Indicated thermal efficiency
LHV	Lower heat value
NG	Natural gas
PRR	Pressure rise rate
SOI	Start of injection
UCH	Unburned hydrocarbon
$Q_{apparent}$	Apparent heat release
M_{H2}	Hydrogen mole fraction
H_2	Hydrogen
IDT_{STD}	Standard deviation of IDT
IDT_{COV}	Coefficient of variation of IDT
$IMEP_{STD}$	Standard deviation of IMEP
$IMEP_{COV}$	Coefficient of Variation of IMEP
V_d	Displaced cylinder volume
$\dot{m}$	Mass flow rate
P_{ratio}	Pilot fuel ratio
STFT	Short-time Fourier transform
T_{air}	Charge-air temperature
TF	Tri-fuel

Greek symbols

$\lambda_{mixture}$	Gaseous fuel lambda
θ	Crank angle degree
ψ	Eigenvectors
γ	Specific heat ratio
θ_{IDT}	Crank angle degree of IDT
θ_{SOI}	Crank angle degree of SOI
ΔP	Bandpass pressure

during the last few years [1,2]. However, there are still no real alternatives that can compete with the ICE over the entire range of applications that they cover, even today, ICEs are undergoing continuous improvements [3–5]. Both natural gas and hydrogen have long been considered alternative fuels for the transportation sector and have fueled vehicles for decades [6]. Particularly, H_2 has been attracted the attention of researchers because of its carbon-free nature and excellent combustion properties. Additionally, it can be produced by using renewable energies. However, using H_2 as a sole fuel in ICEs faces many challenges, including lower volumetric efficiency, pre-ignition, backfire and knocking [6,7]. Therefore, a multi-fuel combustion technology in ICE using H_2 and CH_4 mixtures with pilot diesel, namely TF combustion has been investigated as a promising method for future ICEs [6].

The excellent combustion properties of H_2, such as broader flammable limits, lower ignition energy, higher diffusion rate, faster laminar flame speed, and stronger lean-burn capability, has the potential to effectively improve the combustion efficiency and reduce exhaust emissions [7–10]. Furthermore, the concept has several attractive properties from the research point of view: 1) H_2 addition may shorten the ignition delay, 2) it could reduce the combustion duration, 3) it can improve the combustion stability and reduce the CCV, and hence 4) it may increase the engine efficiency and reduce the emissions.

H_2 as an additive for various fuels has been studied extensively in ICEs (SI and CI engines). For instance, Liu et al. [11] studied the effect of H_2 addition on combustion characteristics and ignition behavior with H_2/CH_4 mixture and single-pilot diesel. The experimental results indicated that adding H_2 shortens the IDT and combustion duration due to its excellent combustion properties. Zhou et al. [12] compared the engine performance and emissions fueled with DF and TF in a diesel engine. They found that the H_2/CH_4 ratio equal to 30%:70% shows the optimized ratio in reducing particulate and NO_x emissions at 70% and 90% loads. Alrazen et al. [13] investigated TF combustion fueled with diesel-CNG-H_2 and compared TF combustion with diesel-CNG and diesel-H_2 DF operations at various air/fuel ratios using numerical simulations. Lower CO/CO_2 and NO emissions performance were observed in the TF engine when compared to DF operation. Mansor et al. [14] investigated the influence of diesel enrichment with H_2 and CH_4 in a direct injection compression ignition (CI) engine at various H_2/CH_4 ratios with CFD simulation. The result showed that the high H_2/CH_4 ratio is useful for improving the engine performance with reduced CO emission, conversely, the low H_2/CH_4 ratio lowers NO emission. Abu-Jrai et al. [15] examined TF (H_2, CNG, conventional diesel) engine on the combustion characteristics, engine emissions, and selective catalytic reduction at low, medium, and high engine loads. Results showed that the H_2 and CNG reduce in-cylinder pressure and heat release rate (HRR) at low load, and considerably increase in the premixed combustion phase at high engine load.

From the above literature [7–15], it can be noted that several studies have examined the positive features of CH_4 enriched with H_2 in DF engines and the outcomes on performance and pollutant emissions. However, there are very few studies that report the combustion stability and CCV in TF engines. Single-cycle combustion stability or CCV in a continuous operation is known to pose a critical role in H_2 enriched TF combustion. Cyclic variations are typically observed in spark ignition (SI) engines due to the changes in the burn rate for each successive cycle [12]. These variations may have numerous root causes, including cyclic variation in the cylinder gas motion and fuel mass flow rate, unscavenged exhaust gases composition, or cyclic variation of the mixture composition near the spark plug, leading to differences in combustion speed or local end-gas autoignition [16–18]. These effects have been studied extensively in the past using experimental [19–21] and numerical tools [18,22–25] Similarly, in pilot-diesel ignited DF or TF combustion, high cyclic variations are expected due to the high influence of small perturbations in temperature and composition on the pilot-diesel autoignition or abnormal combustion e.g., PREMIER combustion or knocking due to end-gas autoignition [26,27].

Significant CCV is less common in conventional DF combustion engines operating at a stoichiometric equivalence ratio. This is due to the nature of the combustion properties of CH_4, which has a relatively low flame speed and high octane number, resulting in stable combustion and less CCV [28]. However, at lean conditions (e.g, $\lambda > 1.6$), the CCV dramatically increases due to the low diffusivity, reactivity, flame propagation speed and burning velocity, and narrow flammability range [29]. The addition of H_2 allows the engine to operate at lean conditions with high combustion stability [30]. Wu et al. [31] investigated the addition of H_2 on engine performance and CCV at various engine loads (0–60%) and EGR coefficient (0–40%), adjusting the share of H_2 energy in the range from 0 to 20%. The combustion CCV was analyzed based on the coefficient of variance in the indicated mean effective pressure (COV of IMEP). The results showed that adding H_2 increases the COV of IMEP from 0.9% to 2.8%. Talibi et al. [32] found that by increasing the H_2 concentration up to 20%, H_2 auto-ignition may lead to abnormal combustion and increased CCV. Tsujimura et al. [33] recorded similar pre-ignition characteristics in a TF engine with 50% of the H_2 energy share. Allenby et al. [34] revealed that the H_2 addition to NG with EGR utilization can greatly extend combustion stability. The existence of H_2 produces a significant reduction in the percentage of COV of IMEP.

Combustion stability and CCV are known to pose a critical role in H_2 enriched TF combustion, however, comprehensive studies on CCV in DF or TF engines have been limited in number. The CCV information derived from cylinder pressure variations can be used to estimate the engine performance and control the combustion [34]. Recent efforts have focused on considering the cycle-to-cycle variability in the realm of nonlinear dynamics and applying chaos-theoretic methods to unravel the nonlinear aspects of these variations. It has also been shown that the variability may be due to a stochastic component [12], and attempts have been made to estimate the noise level [16]. The short-time Fourier transform (STFT) has attracted much attention in recent years because it can be applied to determine the sinusoidal frequency and phase content of local sections of a signal as it changes over time. Compared to the conventional method based on COV of IMEP, the new methods can provide a wealth of information and valuable content of the thermodynamic processes for TF combustion [35]. These methods have been applied in conventional diesel engines for CCV estimation. Stankovic et al. [36] present a time-frequency analysis of multiple resonances with STFT in combustion chamber pressure signals and investigate a procedure to estimate the instantaneous frequencies. Payri et al. [37] analyzed the frequency components of the in-cylinder pressure signal to decompose the in-cylinder pressure evolution according to three phenomena taking place during diesel engine operation: pseudo-motored, combustion and resonance excitation.

However, for the TF combustion, since the combustion process is completely different from the conventional diesel combustion, the size and shape of the window for STFT needs to be selected properly. Owing to the achievable time-frequency resolution of STFT, it is limited by the Heisenberg uncertainty principle and thus, this method cannot be used for CCV estimation. On the contrary, CWT is introduced to overcome the disadvantages of STFT [38]. Wavelet-based techniques are increasingly used for time series analysis in a wide variety of applications. The CWT maps the spectral characteristics of a time series onto a time-frequency plane from which the various periodicities and their temporal variations can be discerned [39–41]. Using a variable-size window in the time-frequency (time-period) plane, the CWT adjusts the time and frequency resolutions adaptively. It uses a window that narrows when focusing on high-frequency components of the time series and widens on low-frequency features, analogous to a zoom lens [42]. Recently, CWT has been applied to the analysis of CCV in gasoline, diesel, and natural gas engines [43,44].

The present study provides a systematic framework for performing TF combustion in a heavy-duty CI engine to clarify the effect of H_2 concentration and charge-air temperature on the combustion stability and cycle-to-cycle variations at a wide range of operating conditions. The present study aims to.

1) Characterize the ignition behavior and engine performance of TF combustion by varying the H_2 concentration (M_{H2} = 10%, 20%, 40%, 60%) and the charge-air temperature (T_{air} = 25 °C, 40 °C, 55 °C),
2) Analyze the combustion stability with short-time Fourier transform (STFT) to assess the knock intensity and the resonant frequency evolution,
3) Apply continuous wavelet transform (CWT) to examine the effect of the pilot fuel properties on the engine CCV.

Experimental setup and operating conditions

Full-metal single cylinder engine

Fig. 1 shows the schematic of the test-engine setup. A single-cylinder CI engine is operated under multiple-fuel modes (e.g., DF or TF). A 45 kW ABB low voltage motor coupled with a frequency convertor (ACS800-11) are adopted to provide the load and control the engine speed. The engine allows monitoring and flexible control of engine operating parameters related to necessary parallel systems, such as electro-hydraulic valve actuation (EHVA), charge-air conditioning, and fuel injection systems. An electrohydraulic valve actuator (EHVA) system is employed to provide a fully flexible variable valve lift and timing for the air-exchange system. The engine is equipped with RHM-08 Coriolis mass flow meters (Rheonik Messtechnik GmbH), for measuring charge-air ($\dot{m}_{air}$) and two EL-FLOW® mass flow meters/controllers, for measuring port-injected CH_4 and H_2 mass flow rates ($\dot{m}_{CH4}$ *and* $\dot{m}_{H2}$), respectively. In this study, the charge-air mass flow rate is 80 kg/h and maintained as the temperature is increased. To get the same air mass flow rate, a PID controller was adopted to adjust the charge air mass flow accordingly. The charge air mass flow measured by a Coriolis mass flow meter and the thermocouple is located at manifold where close to the intake valve. A

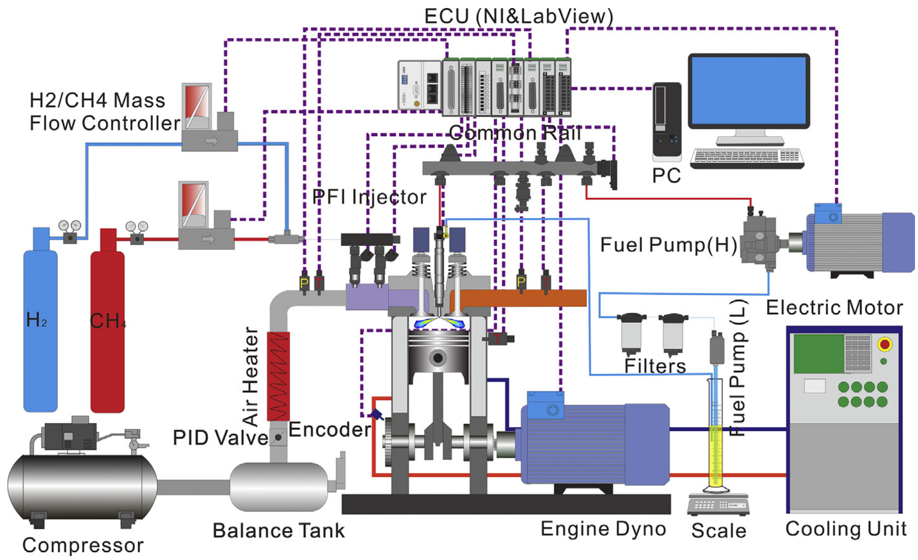

Fig. 1 – Schematic of the test engine setup.

Bosch CRI3 piezo injector (3-hole) is adopted to provide pilot diesel injection with high stability and low delay [45]. Two Bosch natural gas injectors (NGI2) are employed for gaseous fuel injection. The cylinder pressure is measured by a piezo-electric sensor (type 6125C, Kistler Co., Inc.) with a charge amplifier (type 5011B, Kistler Co., Inc.) at a resolution of 0.2 CAD. The crank-angle signal is acquired at a revolution of 0.2°CA with a crank-angle encoder. An external water-cooling system is employed to warm the engine. An engine control unit (ECU) based on the National Instrument field-programmable gate-array (NI-FPGA) is adopted to control and monitor the charge-air mass flow and temperature. More detailed specifications of the test engine is shown in Table 1.

Fuel properties

The properties of the EN590, CH_4, and H_2 are listed in Table 2. The EN590 is utilized as a pilot fuel, which has higher reactivity and lower auto-ignition temperature compared to gaseous fuels, thereby can be easily ignited by compression. CH_4 and H_2 as gaseous fuels premixed with charge air, which can be ignited by the pilot ignition source. The CH_4 and H_2 are provided by AGA Industrial Gases (Finland) with a purity of 99.95% and 99.9%, respectively.

Table 1 – Test engine specifications.

Engine type	4-Stroke modified single-cylinder diesel engine
Bore	111 mm
Stroke	145 mm
Swept volume	1402 cm^3
Combustion bowl	89.8 cm^3
Vol. compression ratio	16.7:1
Swirl ratio	2.7
Pilot injection system	Bosch piezo CRI3 common rail
Injector no. of holes x diameter	3 × 0.160 mm (symmetric)
Pilot injection pressure	1000 bar
Port fuel injection system	2 × Bosch NGI injectors
Valve system	Electrohydraulic valve actuator

Engine operating conditions and experimental matrix

This investigation aims to assess the effect of H_2 concentration (M_{H2}) and charge-air temperature (T_{air}) on ignition behavior, combustion stability and engine performance in a TF combustion engine. Fig. 2 outlines the matrix for investigating the effect of M_{H2} and T_{air} on TF combustion. It should be noted that the test matrix is limited by the knocking, and increasing in M_{H2} or T_{air} beyond the certain limit may produce heavy knocking (based on peak HRR value), enough to cause permanent damage to the engine.

The engine operating conditions are shown in Table 3. In this study, a full metal single-cylinder engine is operated at 1200 rpm with an equivalence ratio of 0.5 ($\varphi = 0.5$) to estimate the effect of H_2 addition on ultra-lean TF combustion. The total energy input into the cylinder is ~130 MJ/h depending on the M_{H2}, which corresponds to the IMEP of 13 bar. The charge-air mass flow is controlled by an air mass flow controller, which is set to 80 kg/h. The pilot injection pressure is 1000 bar, and the pilot diesel energy share ratio is ~10% (P_{ratio} = ~10%) with a constant injection duration. The pilot injection time is 7 CAD BTDC. A total of 200 continuous cycles for each test point are recorded for data analysis.

Operating parameter and data analysis

Before starting the data analysis, the motored cylinder pressure profiles under different M_{H2} conditions are calibrated with a detailed GT-Power model. Fig. 3 illustrates the modeled bulk in-cylinder temperature (T_{bulk}) and specific heat ratio (γ) with different M_{H2} at 298 K. The purpose of this calibration is to estimate the T_{bulk} and γ, which cannot be measured directly. The result indicates that pure charge-air shows a higher γ value than the H_2–CH_4-air mixture, and there is a

Table 2 – Specification of diesel fuel, CH_4 and H_2 [46–48].

Items	Unit	EN590	Hydrogen	Methane
Molecular formula		$C_nH_{1.8n}$	H_2	CH_4
Lower heating value	MJ/kg	≈43.1	120	50
Cetane number		52.6	–	0
Stoichiometric air-fuel ratio		14.5	34.48	17.19
Density at 15 °C, 1 atm	kg/m^3	820–845	0.09	0.725
H/C ratio	mole/mole	1.91	–	4
Viscosity at 40 °C	mm^2/s	2.0–4.5		18.72
Autoignition temperature	°C	250	585	540
Minimum ignition energy	mJ	–	0.02	0.3
Flammability limits (volume% in Air)	%	0.6–5.5	4–75	5–15
Burning velocity in NTP	cm/s	37–43	37–45	265–325
Quenching gap in NTP air	cm	–	0.064	0.203
Diffusivity in air	cm^2/s	~0.07	0.63	0.16
Research octane number		30	130	>122
Specific heat *Cp*	kJ/kgK@300k	2.05	14.89 (gas)	2.226

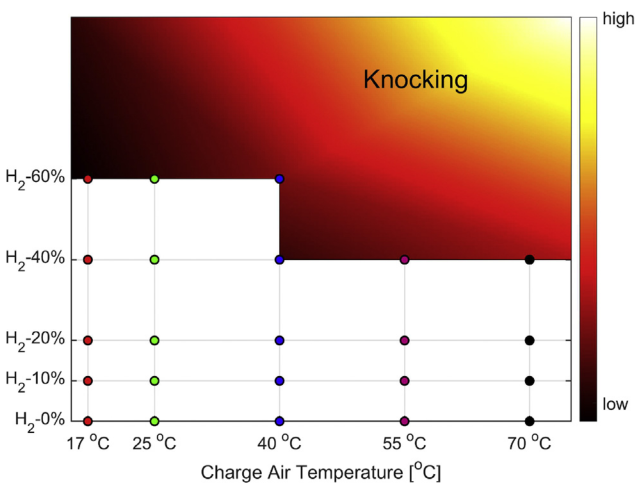

Fig. 2 – Experimental matrix of the effect of M_{H2} and T_{air} on TF combustion.

Table 3 – Overview of the engine operating conditions.

Item	Unit	Value
Engine speed	rpm	1200
SOI	CAD BTDC	7
Pilot injection duration	ms	0.256
$\dot{m}_{air}$	kg/h	80
Equivalence ratio	–	0.5
H_2 mole fraction	mole %	0, 10, 20, 40, 60
Charge-air temperature	°C	17, 25, 40, 55, 70
Pilot energy ratio	%	10
CH_4 energy ratio	%	90, 87.1, 83.7, 74.9, 61.9
H_2 energy ratio	%	0, 2.9, 6.3, 15.1, 28.1
Total energy	MJ/h	123, 127, 131, 133, 136

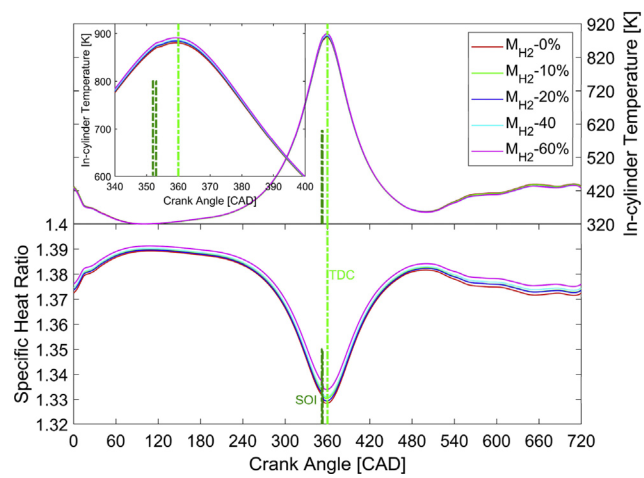

Fig. 3 – Specific heat ratio and bulk in-cylinder temperature at different M_{H2}. The increase of the H2 shows a higher γ value and creates a slightly higher bulk in-cylinder temperature.

huge change of γ during the compression and expansion stroke. The variety of γ may lead to different motored pressures and temperatures at the SOI. For the conventional diesel engine, $\gamma = 1.35$ is usually selected for heat release rate calculation. However, to gain an accurate HRR, a variable γ vs crank angle should be used in DF and TF combustion due to the large gap between the pure charge-air and H_2–CH_4-air mixture in γ. In this study, the γ for different charge mixtures is varied according to the verified GT-Power results.

Definition of the ignition delay time

The estimation of IDT plays a crucial role in TF combustion. The IDT in the current study is defined as the time interval between the start of pilot injection and the start of combustion.

$$IDT = \theta_{IDT} - \theta_{SOI} \tag{1}$$

Normally, the crank angle at 5% or 2% of cumulative heat release, namely CA5 or CA2 is defined as IDT in the conventional diesel engine [49]. However, these IDT definitions are not suitable to the DF and TF combustion due to the combustion rate is not determined by the pilot fuel but by premixed flame propagation. In this study, the pressure rise delay (PRD) is defined as the IDT. Fig. 4 shows ITDs with different definitions. It indicates that PRD shows more reproducible and reliable IDT compared with CA5 and CA2. The coefficient of variation (COV) of IDT is derived to characterize the variation of ignition as below,

$$IDT_{STD} = \sqrt{\frac{1}{n-1}\sum_{n=1}^{200}(IDT_i - IDT_{AVG})^2} \quad (2)$$

$$IDT_{COV} = \frac{IDT_{STD}}{IDT_i} \quad (3)$$

where, IDT_i, IDT_{AVG} are the individual IDT and averaged IDT, respectively. IDT_{STD} is the standard deviation of the IDT. IDT_{COV} is the coefficient of variation of the IDT.

Definition of the combustion states

To estimate the combustion states at different M_{H2} and T_{air} conditions, the pressure rise rate (PRR) is applied to evaluate the pressure oscillations and define the abnormal combustion such as PREMIER combustion and knocking, as shown in Fig. 5. It can be observed that, in normal combustion, the PRR after the main combustion (CA50) is gradually declining. In PREMIER combustion, the PRR shows a small rebounding and apparent peak after CA50. Here, the peak value is comparable to the PRR during the premixed or main combustion. However, in the knocking, the peak of the PRR after CA50 is abrupt and much higher than that of the PRR during the main combustion.

In normal combustion, the declining PRR after CA50 is due to low M_{H2} or T_{air}, which results in a low flame propagation or even quenching at the end of the main combustion [20]. However, an increase in M_{H2} or T_{air} promotes auto-ignition in the end-gas region. This end-gas auto-ignition in a favorable range is called PREMIER combustion mode. When end-gas auto-ignition exceeds a favorable range due to an increased M_{H2} or T_{air} beyond a specific level, this creates multiple flame fronts and generates an extremely high PRR [26,27], which leads to engine knocking.

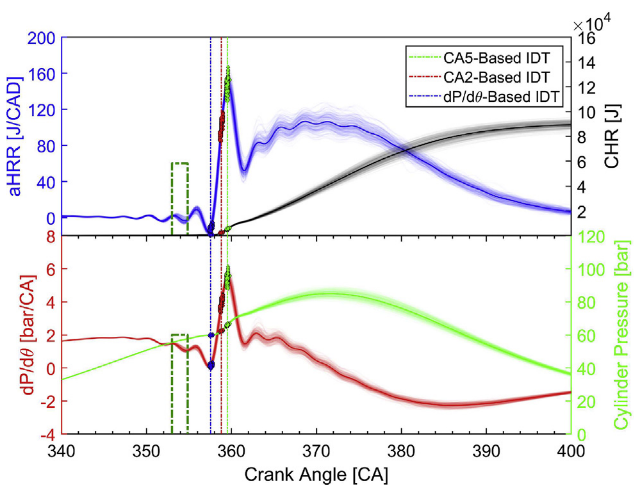

Fig. 4 – Representative in-cylinder pressure, dP/dθ, HRR, CHR, and different definitions for IDTs. dP/dθ-based IDT is defined as the pressure rise delay which represents the start of combustion. CA2 and CA5 are defines as 2% and 5% of the total cumulative heat release. CA2 and CA5 based IDT can be observed during premixed combustion, which cannot represent real IDT properly compared to dP/dθ-based IDT.

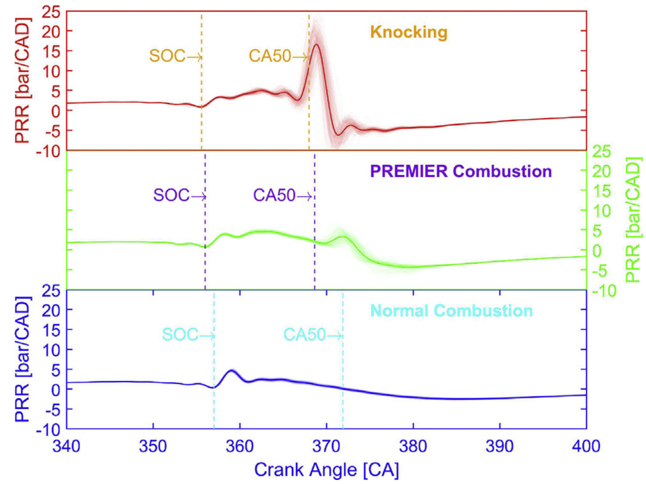

Fig. 5 – Definition of combustion states based on the PRR. Normal combustion (bottom) shows declining PRR after CA50; PREMIER combustion (middle) exhibits a small rebounding and an apparent peak after CA50; Knocking (top) exhibits an extremely high PRR right after CA50.

Short-time fourier transform -STFT

In recent years, the short-time Fourier transformation (STFT) has attracted much attention because it can be applied to determine the sinusoidal frequency and phase content of local sections of a signal as it changes over time. Here, in this study. STFT time-frequency method is implemented to determine single-cycle combustion stability. It extracts the frequency content of an in-cylinder pressure signal while preserving the time signal events. The STFT algorithm windows a small segment of the time series waveform and applies a Discrete Fourier Transform (DFT) on the data contained in the window [50]. The result is a set of data representing the signal's energy signature in frequency and time. Windows represent weighting functions, which aim to reduce the order of discontinuity at the boundary of the finite observation interval, are applied to data to reduce the effect of the spectral leakage when dividing the signal ($s_t(\varnothing) = s(\varnothing)\omega(\varnothing - \alpha)$). In this study, the STFT method is applied to estimate the combustion stability in an individual cycle. The STFT applies a window function at various locations and performing a Fourier transform to analyze its frequency content, such as:

$$P_{STFT}(\alpha, f) = |S_t(f)| = \left|\sum_{\varnothing=-\infty}^{\varnothing=\infty} s(\varnothing)\omega(\varnothing-\alpha)e^{-j2\pi f t(\varnothing)}\Delta t(\varnothing)\right| \quad (4)$$

where $\omega(\varnothing)$ is the window function, here, the Blackman-Harris window is designed to reduce spectral leakage. $s(\varnothing)$ is the bandpass pressure (the signal to be transformed). $P_{STFT}(\alpha, f)$ is essentially the Fourier transform of $s(\varnothing)\omega(\varnothing - \alpha)$, a complex function representing the phase and magnitude of the signal over time and frequency. Often phase unwrapping is employed along with either or both the time axis, α , and frequency axis, f, to suppress any jump discontinuity of the phase result of the STFT. The time index α is normally considered to be "slow" time and is usually not expressed in as high resolution as time t. The length of the window is always a trade-off between frequency and time resolution.

Continuous wavelet transform –CWT

Since TF combustion processes are completely different from conventional diesel combustion, the size and shape of the STFT window function require a precise implementation. Moreover, the time-frequency resolution generated by STFT is limited by the Heisenberg uncertainty principle, which prevents the correct estimation of CCV in a continuous operation. Therefore, continuous wavelet transform (CWT) is introduced here to overcome the disadvantages of STFT. CWT maps the spectral characteristics of a time series onto a time-frequency (time-period) plane from which the various periodicities and their temporal variations can be discerned by visual inspection [39–41]. It uses a variable-size window in the time-frequency (time-period) plane, which adjusts the time and frequency resolutions adaptively. Additionally, an adaptive window function has applied that narrows when focusing on high-frequency components of the time series and widens on low-frequency features, analogous to a zoom lens [42].

In this study, the CWT method is adopted to create the WPS and global power spectrum (GPS) from the time series of IMEP. CWT can construct a time-frequency representation of a time series that offers convincing time and frequency localization, so it can analyze localized intermittent periodicities of the CCV in the engine. In practice, CWT is estimated by applying the frequency-domain fast algorithm to IMEP time-series in Matlab. In time series IMEP, due to the similar resolution in both time and frequency, a complex Morlet wavelet consists of a plane wave modulated by a Gaussian function and is described by Ref. [43]:

$$\psi_0(t) = \pi^{-1/4} e^{i\omega_0 t} e^{-t^2}/2 \quad (5)$$

where ω_0 is the one-dimensional frequency taken as $\omega_0 = 2500$ Hz throughout this paper for the Morlet wavelet. Let f be a continuous time series. Then the wavelet transform of f is defined as

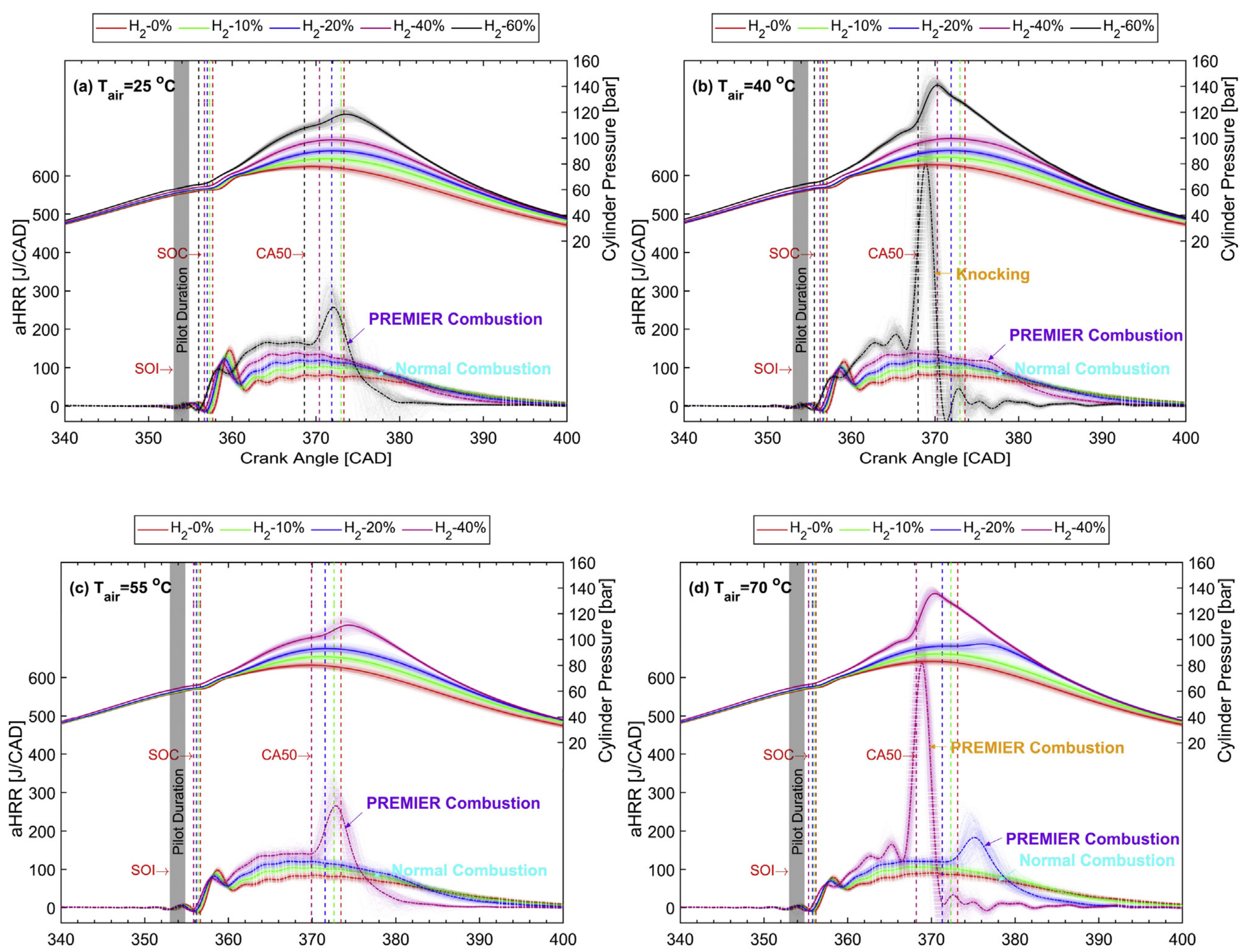

Fig. 6 – Effect of M_{H2} on the TF combustion at different T_{air}, (a) 25 °C, (b) 40 °C, (c) 55 °C, (d) 70 °C. The normal combustion gradually transits to abnormal combustion such as PREMIER combustion and knocking with the increase of the H_2 concentration or/and charge-air temperature due to the end-gas auto-ignition.

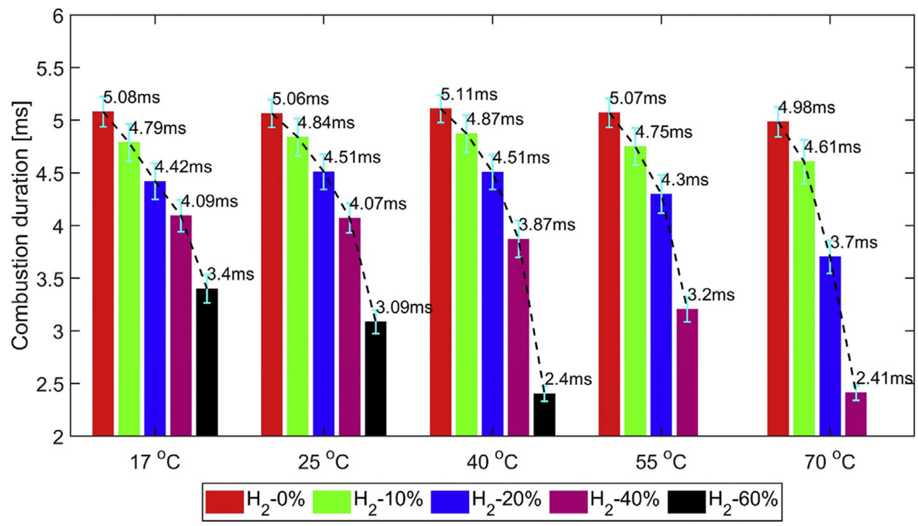

Fig. 7 – Comprehensive comparison of combustion duration at different M_{H2} and T_{air}. It is noted that the addition of the H_2 proportionally reduces the combustion duration at all charge-air temperature conditions. The charge-air temperature shows an insignificant effect on the combustion duration in normal combustion mode.

$$W_f(a,b) = \frac{1}{\sqrt{a}} \int_{-\infty}^{\infty} f(t)\overline{\psi_0\left(\frac{t-b}{a}\right)}dt(a>0, b \in R) \quad (6)$$

where the overbar denotes a complex conjugate. We call $|W_f(a,b)|^2$ the wavelet power spectrum of f. For the discrete-time series $\{x_n\}_0^{N-1}$ of time step δt, its wavelet transform is defined as

$$W_n(s) = \sqrt{\frac{\delta t}{s}} \sum_{n'}^{N-1} x'_n \overline{\psi_0\left[\frac{(n'-n)\delta t}{s}\right]} \quad (7)$$

where $|W_n(s)|^2$ the wavelet power spectrum of $\{x_n\}_0^{N-1}$. The wavelet transform is very useful for time series analysis where smooth, continuous variations in wavelet amplitude are expected.

Results and discussion

This section is divided into three subsections. Section Effect of H_2 on ignition characteristics and engine performance characterizes the effect of H_2 concentration and charge-air temperature on the characteristics of aHRR, IDT, IMEP, COVs and ITE. Section Combustion stability based on STFT quantifies the effect of M_{H2} and T_{air} on the combustion stability in an individual cycle based on the STFT. Section Cycle-to-cycle variations based on CWT estimates the effect of M_{H2} and T_{air} on the CCV based on the CWT.

Effect of H_2 on ignition characteristics and engine performance

Fig. 6 (a)–(d) illustrates the effect of M_{H2} on the in-cylinder pressure and aHRR under different T_{air} (17 °C–70 °C) conditions. It should be noted that the results under cold conditions (T_{air} = 17 °C) are not shown for brevity. The results indicate that the addition of the H_2 increases the in-cylinder pressure and aHRR. This can be explained, on the one hand, increasing M_{H2} leads to a slight increase in the total energy because of the high LHV of the H_2 when keeping the equivalence ratio constant (φ = 0.5), as shown seen in Table 3. On the other hand, the addition of the H_2 also increases the combustion efficiency due to its excellent combustion properties, such as broader flammable limit, lower ignition energy, higher diffusion rate, faster laminar flame speed, and stronger lean-burn capability [8–11].

At low T_{air} conditions as shown in Fig. 6(a), the addition of the H_2 shortens the IDT, CA50 and combustion durations. The abnormal combustion starts at M_{H2} = 60% and T_{air} = 25 °C where an abnormal aHRR peak after the main combustion can be defined as PREMIER combustion due to the end-gas auto-ignition [26,27]. The PREMIER combustion occurs with auto-ignition in the end-gas region when the main combustion

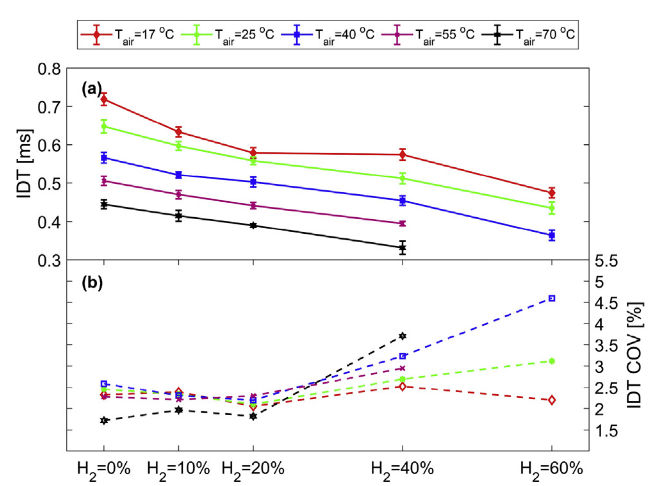

Fig. 8 – Effect of M_{H2} on the (a) ITDs, (b) IDT COVs at different T_{air}. The result indicates that increasing M_{H2} or T_{air} leads to a shorter IDT but higher IDT variations.

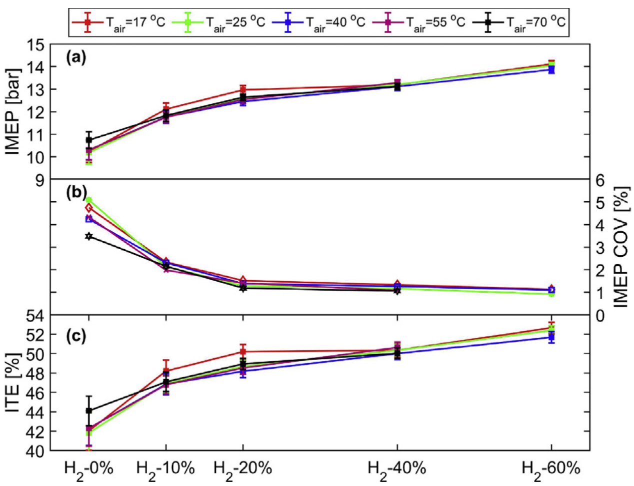

Fig. 9 – Effect of M_{H2} on the (a) IMEP, (b) IMEP COV and (c) ITE at different T_{air}. It is noted that increasing M_{H2} results in a higher IMEP and ITE, as well as lower COV of IMEP.

flame propagation is nearly finished. Auto-ignition is triggered by the increase of the in-cylinder pressure and temperature when M_{H2} is high. Fig. 6(b) shows the TF combustion at $T_{air} = 40$ °C with varying the H_2 concentration. The addition of the H_2 exhibits a similar effect on IDT, CA50 and combustion durations with a lower charge-air temperature. However, an extremely strong abnormal aHRR peak can be observed right after CA50. Similarly, this strong pressure rise caused by end-gas auto-ignition is defined as knocking. In knocking mode, heat is released in two stages when the engine undergoes this type of combustion.

With further increasing the T_{air} to 55 °C as shown in Fig. 6(c), the PREMIER combustion can be observed when $M_{H2} = 40\%$ and the higher H_2 concentration case cannot proceed due to heavy knocking. Fig. 6(d) depicts the effect of the M_{H2} at high T_{air} condition ($T_{air} = 70$ °C). The high charge-air temperature dramatically promotes the combustion process, resulting in a shorter IDT, CA50, and combustion duration compared to the lower T_{air} conditions. Additionally, the increase of the charge-air temperature reduces the tolerance of the H_2 addition in normal combustion, which exhibits the PREMIER combustion at $M_{H2} = 20\%$ and knocking at $M_{H2} = 40\%$ conditions.

Overall, the increase of the charge-air temperature and H_2 concentration, resulting in a combustion transition. With increasing the T_{air} and/or M_{H2} the normal combustion gradually transits to PREMIER combustion, then transits to knocking due to the faster flame speed and wider flammability of the gaseous mixture with increasing T_{air} or M_{H2}, which creates a faster auto-ignition burning rate and induces a sudden pressure rise between the premixed flame and end-gas flame. Subsequently, inducing strong pressure oscillations during main combustion. This process also dramatically reduces the IDT, CA50 and combustion duration.

The effect of M_{H2} on the IDT, CA50, and combustion duration are shown in Figs. 6 and 7. Increasing M_{H2} leads to a shorter IDT, CA50, and combustion duration at all T_{air}. On the one hand, increasing M_{H2} results in a faster burning rate due to its excellent combustion properties (e.g., fast flame speed and board flammability limits), thereby shortening the CA50 and combustion duration. On the other hand, the addition of the H_2 leads to a higher in-cylinder temperature, subsequently induces the end-gas auto-ignition, which results in abnormal combustion (e.g., PREMIER and knocking).

The abnormal combustion can shorten the combustion duration dramatically due to the main combustion and end-gas burning take place simultaneously. Fig. 7 shows that the addition of the H_2 significantly reduces the combustion duration, especially in knocking mode (e.g., $M_{H2} = 60\%$ and $T_{air} = 40$ °C), the combustion duration is less than half of the normal combustion (e.g., $M_{H2} = 0\%$ and $T_{air} = 40$ °C). However, the T_{air} shows an insignificant effect on the combustion duration at low M_{H2}. With increasing H_2 concentration, the charge mixture shows more sensitivity to the T_{air} due to the combinative effect of the increase of the H_2 concentration and charge-air temperature on the in-cylinder temperature, which may enhance the end-gas auto-ignition. It is noted that the increase of the T_{air} shows a marginal effect on the combustion duration in normal combustion (e.g., $M_{H2} \leq 20\%$). However,

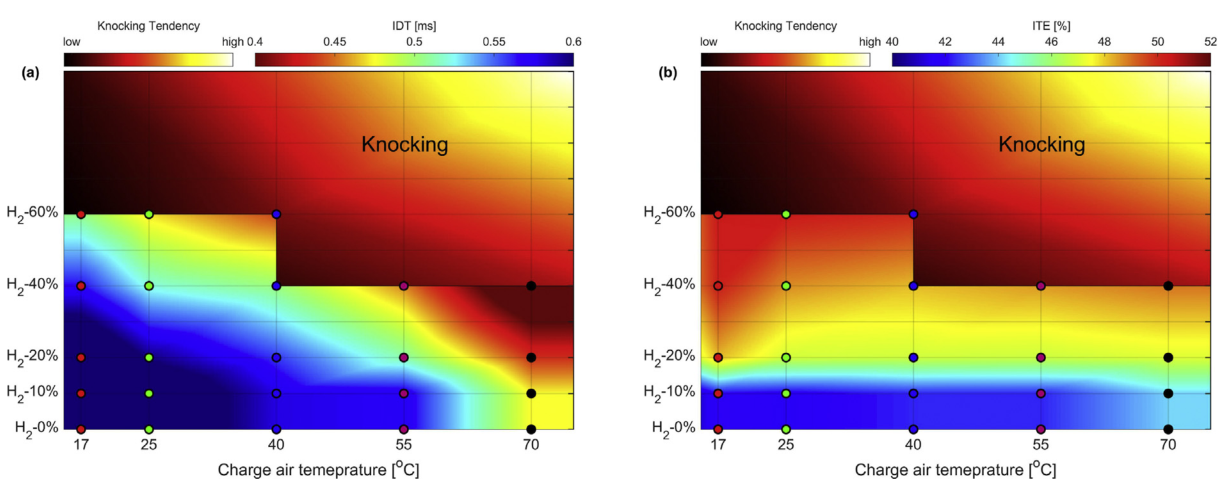

Fig. 10 – Comprehensive comparison of (a) IDT, (b) ITE at different M_{H2} and T_{air} conditions. It is indicated that increasing M_{H2} or T_{air} shortens the IDT as much as 33%. Increasing M_{H2} also improves the ITE up to 10%.

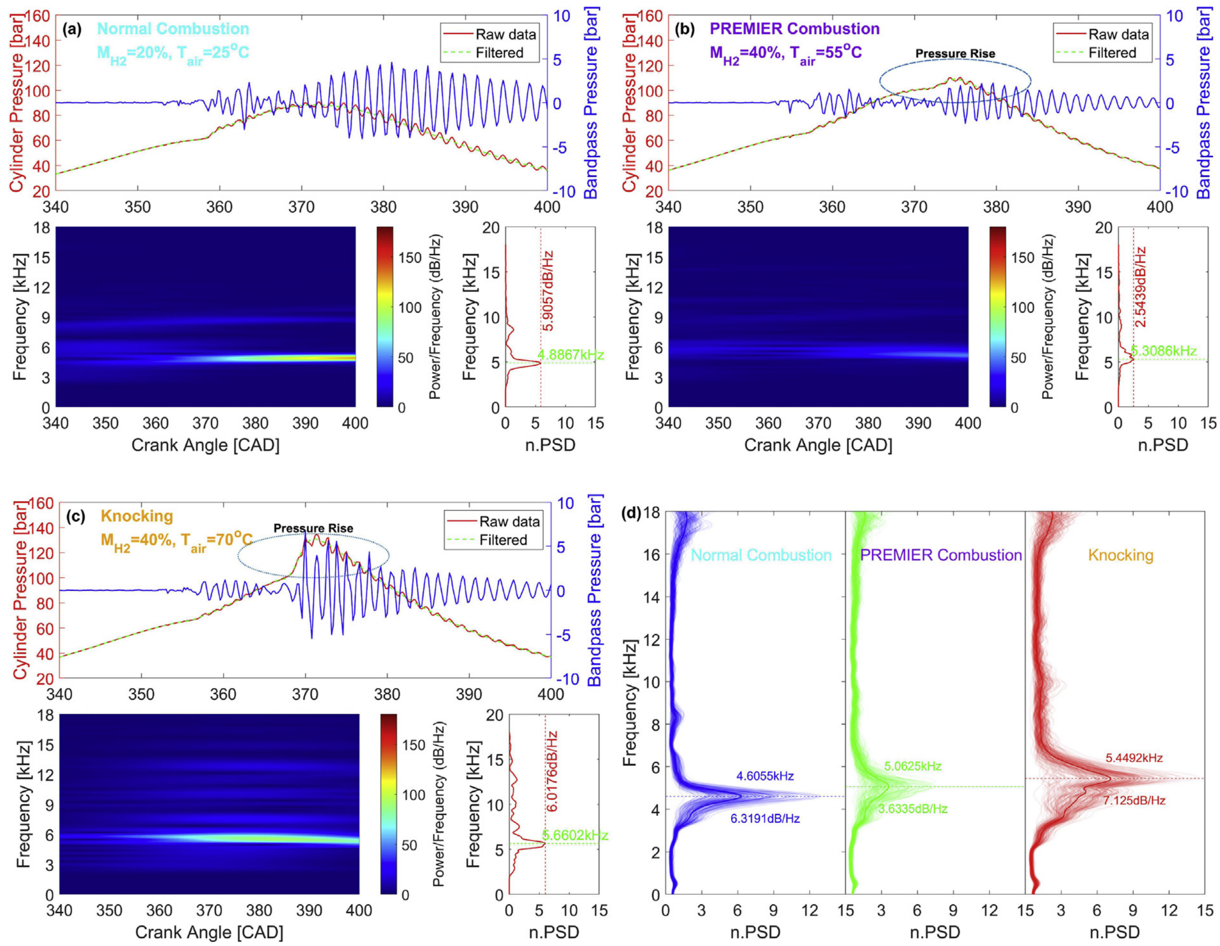

Fig. 11 – The resonant frequency and intensity at different combustion states, (a) normal, (b) PREMIER, (c) knocking, (d) averaged PSD comparison. It is noted that PREMIER combustion exhibits the lowest pressure oscillation intensity which represents the highest combustion stability compared to normal combustion and knocking.

the increase of the T_{air} significantly reduces the combustion duration in abnormal combustion (e.g., $M_{H2} \geq 40\%$). It is worth noting that, when $T_{air} < 55$ °C, the maximum H_2 addition can achieve 60%. However, when $T_{air} \geq 55$ °C, the maximum H_2 addition is 40% due to the appearance of the heavy knocking which may lead to serious damage to the engine.

It is well known that the H_2 addition can accelerate the combustion rate. However, the effect of M_{H2} on IDT is still unclear. Fig. 8 demonstrates the comparison of the effect of M_{H2} on IDTs at different T_{air}. Interestingly, the increase of the M_{H2} shortens IDT, which represents an opposite trend with the previous simulation results in Refs. [51,52]. It is worth noting that this phenomenon appears in a wide charge-air temperature range (17 °C–70 °C), which hints that these opposite trends in IDTs are not caused by the change of the T_{air}. The hypothesis of this opposite phenomenon between the real engine and chemical kinetics simulation is related to the difference of the bulk in-cylinder temperature. In real engines (operating continuously), increasing the M_{H2} leads to a higher accumulative bulk in-cylinder temperature at SOI due to the higher combustion temperature with H_2 addition, which may shorten the IDT. However, in simulation, the temperature at SOI is defined by the users rather than determined by accumulative combustion temperature. Fig. 8(a) shows the effect of M_{H2} on the COV of IDT. At lower M_{H2} and T_{air} ($M_{H2} \leq 20\%$ and $T_{air} < 70$ °C), increasing M_{H2} leads to a lower ignition variation. However, further increasing M_{H2} ($M_{H2} > 20\%$), a dramatic increase in ignition variation (COV of IDT) can be observed. This is because the addition of H_2 increases the bulk in-cylinder temperature due to the fast combustion rate compared with CH_4. The high temperature at the SOI greatly improves the reactivity of the pilot diesel, which leads to high ignition variations (COV of IDT) as shown in Fig. 8(b).

Fig. 9 (a)–(c) shows the effect of M_{H2} on IMEP, COV of IMEP and ITE at different T_{air}. Fig. 9 (a) and (b) depict that adding H_2 leads to a higher IMEP and lower COV of IMEP. As the above explanation, increasing M_{H2} results in higher total energy, combustion efficiency and shorter combustion duration, leading to higher thermal efficiency and less CCV due to its excellent combustion properties. It can be observed in Fig. 9 (c) that the ITE increases ~10% from $M_{H2} = 0$–60%. It should be noted that, in DF mode ($M_{H2} = 0$), the low ITE can be attributed to the ultra-lean ($\varphi = 0.5$) condition which leads to incomplete combustion. Increasing the M_{H2} extends the lean-burn limit and accelerates the combustion rate, which leads to higher combustion efficiency compared to lower H_2 content. Additionally, the addition of H_2 also contributes to combustion stability, which shows a lower COV of IMEP (see in Fig. 9(b)). This is because the addition of H_2 extends the stretch extinction limit, and thus may improve the lean premixed flame stability [34]. However, when M_{H2} > 20%, further increasing the M_{H2} exhibits less sensitivity to the COV of IMEP.

The comprehensive comparison of the effect of M_{H2} and T_{air} on the TF combustion are summarized in Fig. 10 (a). It shows that either increasing the M_{H2} or T_{air} leads to a shorter IDT. This is because increasing the T_{air} leads to a higher bulk in-cylinder temperature at SOI, thereby shortening the IDT. Similarly, increasing the M_{H2} leads to a higher combustion temperature and an accumulative bulk in-cylinder temperature, which also creates a higher temperature at SOI and shortens the IDTs. Additionally, the addition of the H_2 improves the heat capacity of the charge mixture, which also slightly increases the bulk in-cylinder temperature as shown in Fig. 3. Fig. 10 (b) depicts the effect of M_{H2} and T_{air} on engine performance. It is observed that increasing M_{H2} leads to a higher ITE due to the addition of the H_2 extending the flammability limits of the H_2–CH_4 mixtures and improving combustion efficiency. Additionally, the addition of the H_2 shortens the combustion duration, which can also improve the thermal efficiency. It should be noted that increasing T_{air} shows an insignificant or negative effect on TF combustion. This is because increasing T_{air} exhibits an insignificant effect on combustion efficiency but reduces combustion stability (when keep the charge-air mass flow and equivalence ratio constant). Furthermore, if the T_{air} or M_{H2} exceeds a specific level (e.g., T_{air} > 70 °C or/and M_{H2} > 60%) it may lead to heavy knocking.

Combustion stability based on STFT

Next, the STFT method is applied to estimate the combustion stability in an individual cycle. Fig. 11(a)–(c) illustrates the resonance phenomenon of a single cycle (cycle No. 50) at different combustion states (normal, PREMIER and knocking). In each figure (e.g. Fig. 11(a)), the top plot presents the filtered cylinder pressure (green color) and the unfiltered cylinder pressure (red color). The blue line represents bandpass pressure defined as the difference between unfiltered and filtered

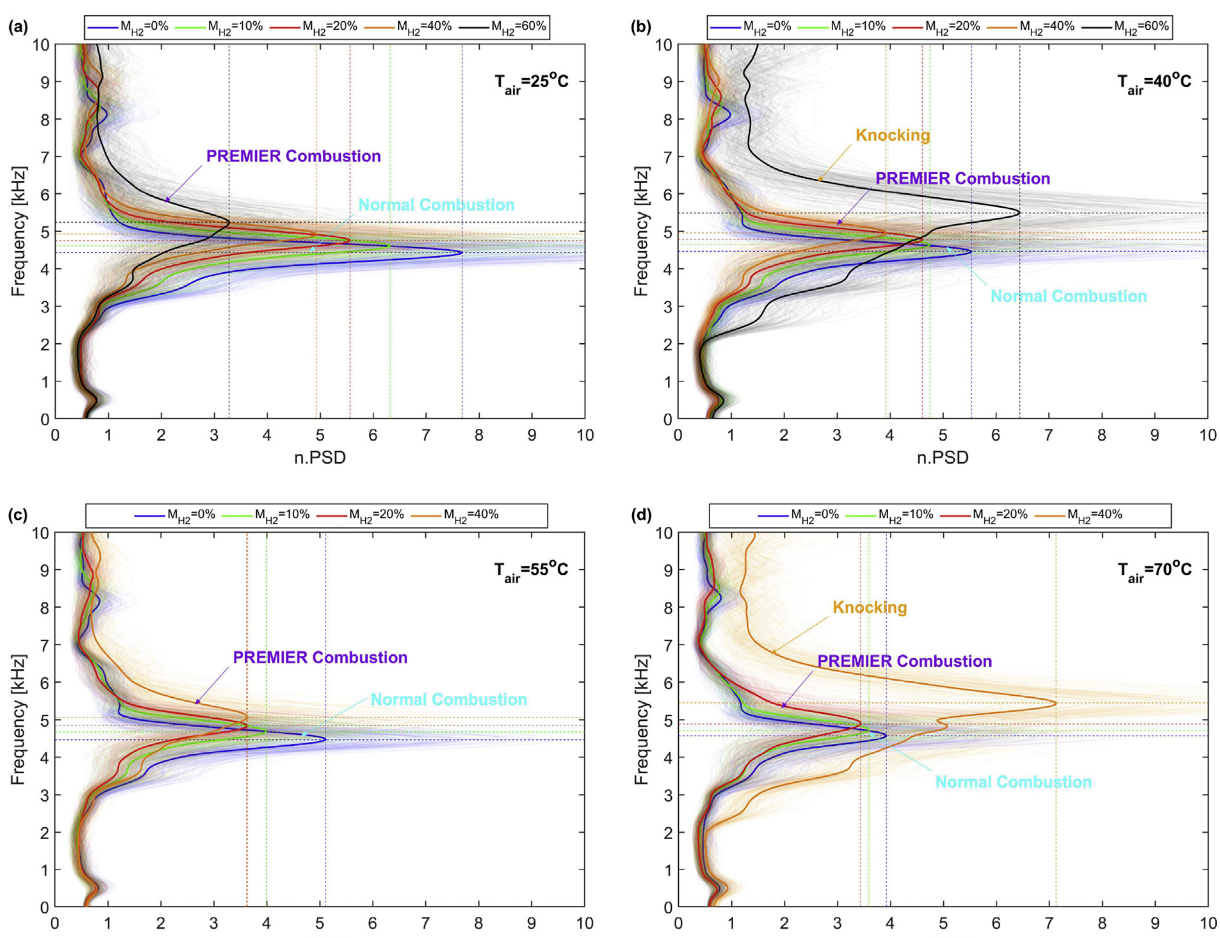

Fig. 12 – Effect of the M_{H2} on combustion stability at different T_{air}, (a) 25 °C, (b) 40 °C, (c) 55 °C, (d) 70 °C. The higher resonant frequency but lower intensity can be observed with increasing the M_{H2} or T_{air} in normal and PREMIER combustion modes, which represents that the addition of the H_2 or the increase of the charge-air temperature improves the combustion stability in normal and PREMIER combustion modes. However, when PREMIER combustion transits to knocking, a wide resonant frequency band and extremely strong pressure oscillation intensity can be observed due to the violate end-gas auto-ignition.

cylinder pressure. The contour plot (lower-left) illustrates resonant frequency and intensity based on the bandpass pressure using STFT. The plot is laid out for a crank angle, while the color shades represent the varying magnitude of the frequency component. The power spectral density (PSD) is a summarized fluctuation power at each frequency and it is presented in the plot at the lower-right corner. The cyclic (transparent curves) and averaged (solid curves) PSD of all combustion states are illustrated in Fig. 11(d).

Fig. 11(a) demonstrates resonance phenomenon in normal combustion mode (M_{H2} = 10% and T_{air} = 25 °C). In this case, the combustion shows higher bandpass pressure oscillations after 370 CAD (tail combustion), which represents more unstable combustion at the end of the main combustion due to the depletion of the H_2/CH_4 mixture. In PREMIER combustion mode, the appearance of the end-gas autoignition leads to a small pressure rise at the end of the main combustion, as shown in Fig. 11(b). Nevertheless, a very smooth bandpass pressure can be found after premixed combustion (364–374 CAD) due to the addition of the H_2 that accelerates the flame propagation and broaden the flammability limits. In knocking mode (see Fig. 11(c)), a high PRR during the main combustion exhibits an extremely strong pressure oscillation.

Fig. 11(d) depicts the individual and averaged distribution of the resonant frequency and the oscillation intensity at different combustion states. In normal combustion mode, two peaks in PSD at a frequency of 4.89 kHz and 8.46 kHz can be observed, which represents the low-frequency oscillation at tail combustion and high-frequency oscillation at premixed and main combustion. The former shows higher oscillation intensity (5.9 dB/Hz) due to lean mixture with low H_2 addition, which leads to flame quenching. The PREMIER combustion shows lower oscillation intensity, but higher resonant frequency compared to normal combustion. This is related to the faster and smoother combustion with H_2 addition, which accelerates the flame propagation and extends the flammability limits. In knocking mode, a broadband resonant frequency (5.66 kHz) with high oscillation intensity (7.125 dB/kHz) can be observed right after premixed combustion. The above-mentioned phenomenon has been proposed to originate from the combined effects of the increased H_2 addition and charge-air temperature, which accelerates the flame propagation, shortens the end-gas auto-ignition timing, and creates multiple flame fronts, which results in a strong pressure oscillation [26,27].

Fig. 12(a)–(d) depicts the effect of M_{H2} and T_{air} on combustion stability based on STFT analysis. In normal and PREMIER combustion, adding H_2 leads to a larger resonant frequency but lower oscillation intensity, which implies that the addition of H_2 accelerates the combustion rate and leads to smoother combustion. However, in knocking mode (see Fig. 12(b)–(d)), the high H_2 content and T_{air} promotes the end-gas auto-ignition and induces a broader resonant frequency (2 kHz–7 kHz), as well as a very strong pressure oscillation (6–7 dB/Hz).

To provide a quantitative assessment for combustion stability, Fig. 13 and Fig. 14 summarize the quantitative effect of M_{H2} and T_{air} on peak pressure oscillation frequency and intensity based on the STFT analysis. As the aforementioned explanation, either increasing the H_2 concentration or charge-air temperature leads to a higher pressure oscillation frequency as shown in Fig. 13, in particular, the addition of the H_2 exhibits more sensitivity to the pressure oscillation frequency. This can be explained by the addition of the H_2 improves the combustion properties of the charge mixtures, which results in a faster flame speed, thereby creating a higher pressure oscillation frequency. Fig. 14 summarizes the effect of M_{H2} and T_{air} on pressure oscillation intensity, which corresponds to combustion stability. The results reveal that increasing H_2 concentration or charge-air temperature leads to a lower

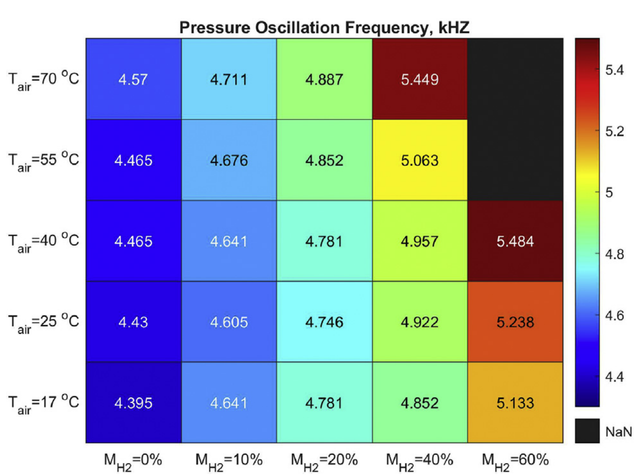

Fig. 13 – Effect of M_{H2} and T_{air} on the pressure oscillation frequency. The larger number (red) shows a higher peak pressure oscillation frequency. Increasing the M_{H2} or T_{air} improves the peak pressure oscillation frequency due to its contribution to the flame propagation. (For interpretation of the references to color in this figure legend, the reader is referred to the Web version of this article.)

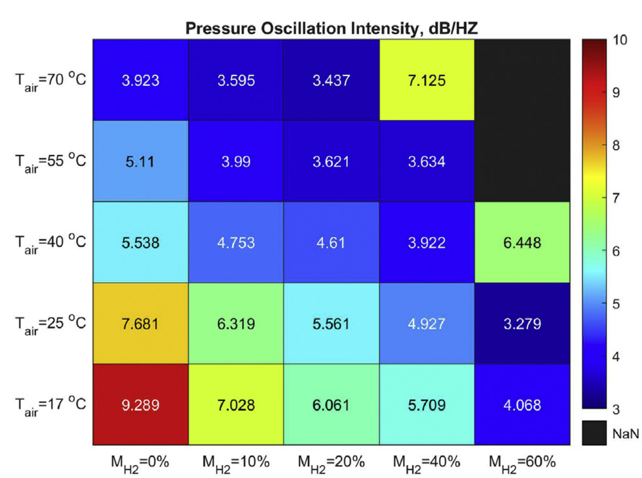

Fig. 14 – Effect of MH2 and Tair on pressure oscillation intensity. The larger number (red) shows a higher peak pressure oscillation intensity. In normal and PREMIER combustion modes, increasing the MH2 or Tair decreases the pressure oscillation intensity which corresponds to an improvement in combustion stability. (For interpretation of the references to color in this figure legend, the reader is referred to the Web version of this article.)

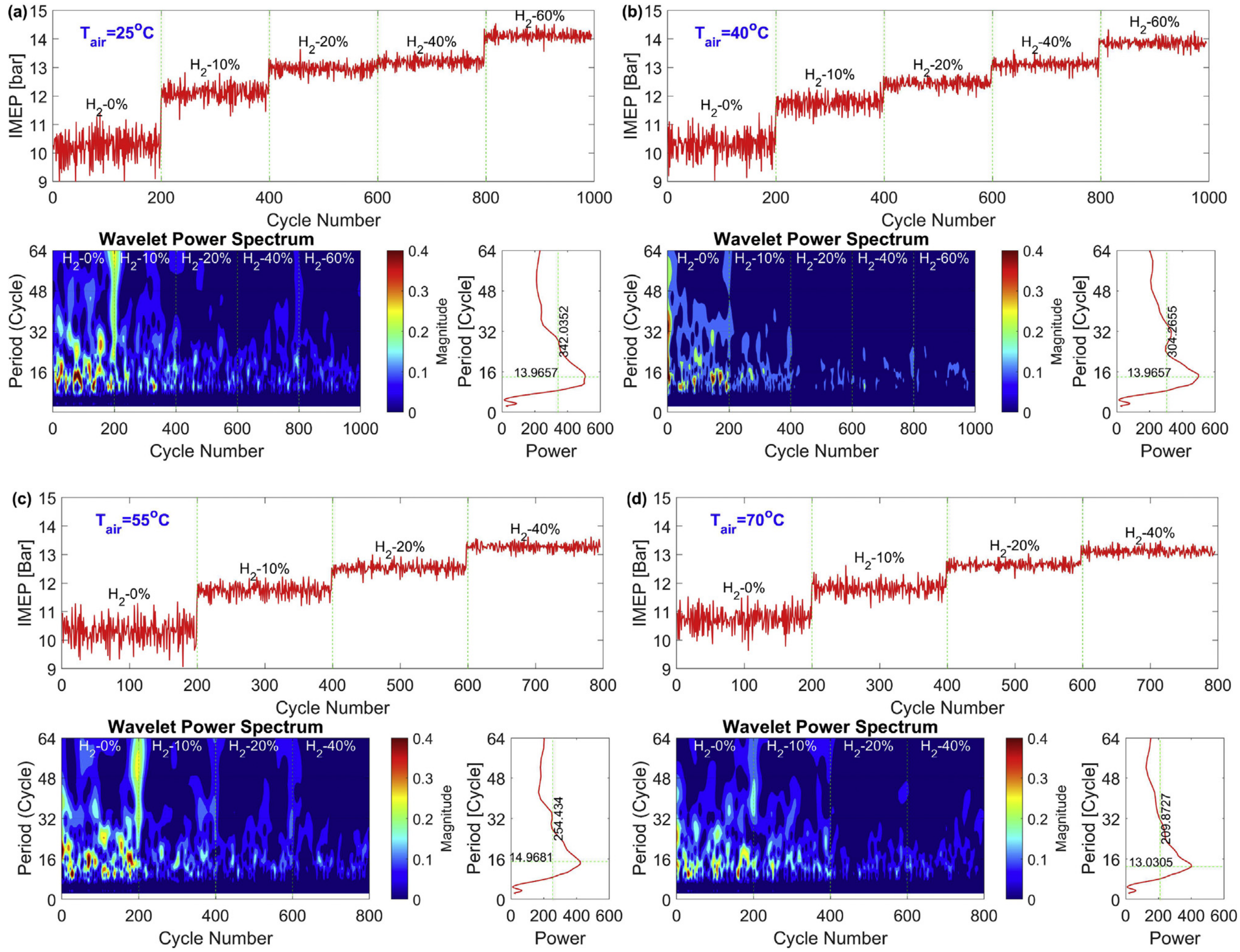

Fig. 15 – Effect of the MH2 on the CCV at different Tair, (a) 25 °C, (b) 40 °C, (c) 55 °C, (d) 70 °C. The high CCV level from low to high is shown as blue to red. It indicates that increasing the MH2 dramatically decreases the CCV level at all charge-air temperature conditions. (For interpretation of the references to color in this figure legend, the reader is referred to the Web version of this article.)

pressure oscillation intensity, which represents higher combustion stability. The interpretation is related to the higher reactivity of the charge mixture with increasing the H_2 concentration or charge-air temperature. However, it is noted that when the H_2 concentration or charge-air temperature exceeds a specific level (e.g., M_{H2} > 40% and Tair>55 °C), the occurrence of the knocking may lead to a higher pressure oscillation intensity.

Cycle-to-cycle variations based on CWT

Here, we aim to estimate the global CCV in TF combustion engines. The time series IMEP and CCV based on CWT at different T_{air} at varying M_{H2} (0%, 10%, 20%, 40%, 60%) are shown in Fig. 15(a)–(d). In each figure, the IMEPs at different M_{H2} conditions are combined from low to high (top). The contour plot shows the distribution of the wavelet power spectrum (WPS) (bottom left). A color bar represents the variation level. In WPS, it is assumed that the IMEP time series has a mean spectrum. If a peak of WPS is significantly above this background spectrum, then it can be considered a true feature of the time series [27]. The integrated WPS value at each cycle period is applied to estimate the global CCV (bottom right).

Fig. 15(a) illustrates the CCV features at T_{air} = 25 °C. It indicates that increasing H_2 concentration lowers the CCV level. Even adding 10% H_2, the wavelet spectrum power is distinctly lower than that in the DF mode. However, when $M_{H2} \geq 20\%$, further increasing the H_2 content shows an insignificant effect on CCV. Similar trends also can be observed at a higher T_{air}. As explained in Section Combustion stability based on STFT, this is can be explained by the addition of the H_2 improves the combustion stability and extends the flammability limits when the charge mixture with low H_2 content, which results in dramatic improvements in CCV. However, when M_{H2} exceeding a specific level (e.g. $M_{H2} \geq 20\%$) depending on the

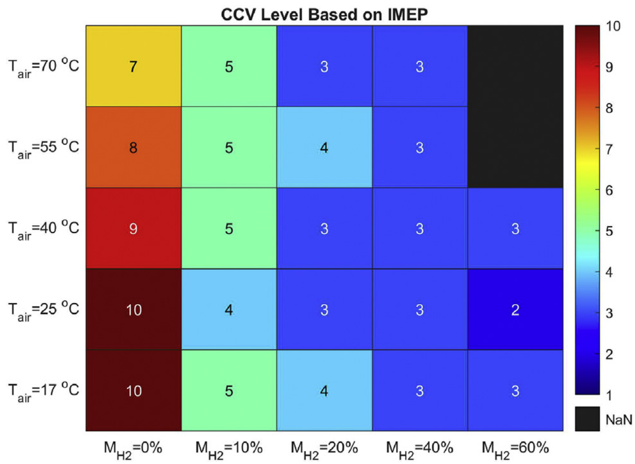

Fig. 16 – Effect of MH2 and Tair on the CCV. The effective wavelet power spectrum based on IMEP is summarized and cataloged to estimate the CCV level from 1 to 10, corresponding to the CCV level from low (blue) to high (red). It is shown that increasing the MH2 or Tair decreases the CCV level. (For interpretation of the references to color in this figure legend, the reader is referred to the Web version of this article.)

charge-air temperature, the addition of the H_2 exhibits less contribution to the combustion efficiency. The lowest CCV features can be observed at $T_{air} = 40$ °C, as shown in Fig. 15(b). Especially, when $M_{H2} \geq 20\%$, the intermittent low power wavelet spectrum can be observed in the low-frequency band of around the 10- cycle period. However, these periodicities do not persist long enough to be considered true oscillations. Further increasing the T_{air} to 55 °C and 70 °C exhibit a high-level of CCV compared to $T_{air} = 25$ °C when $M_{H2} \geq 20\%$. This result can be explained by the abnormal combustion induced by the end-gas auto-ignition such as PREMIER combustion and knocking. Although the PREMIER combustion can improve combustion stability in an individual cycle, the cyclic variations caused by uncontrollable end-gas auto-ignition may increase the CCV level.

To assess the effect of M_{H2} and T_{air} on CCV level, the effective wavelet power spectrum based on IMEP is summarized and cataloged to estimate the CCV level from 1 to 10, corresponding to the CCV level from low to high as shown in Fig. 16. As the above interpretation, either increasing H_2 concentration or charge-air temperature reduces the CCV level. However, when H_2 concentration exceeding a specific level depending on the charge-air temperature (e.g. $M_{H2} \geq 20\%$, $T_{air} \leq 40$ °C), a further increase of the H_2 shows an insignificant effect on the CCV level.

Conclusions

This study aimed at characterizing the effect of M_{H2} and T_{air} on ignition behavior, combustion stability and CCV in a TF combustion engine. The combustion states (e.g., normal, PREMIER and knocking) are well defined under certain conditions (e.g., $\varphi = 0.5$, charge-air mass flow = 80 kg/h). The main findings of this work are:

(1) Increasing the H_2 content and the intake temperature leads to a shorter IDT. The results indicate that increasing the H_2 content from 0% to 60% decreases the IDT by 33% depending on the charge-air temperature. Increasing the intake temperature from 17 °C to 70 °C decreases the IDT by 30%.
(2) Increasing the H_2 content leads to a shorter combustion duration. When increasing the H_2 content from 0% to 60%, the combustion duration is decreasing by 30–50% depending on the intake temperature.
(3) The addition of the H_2 leads to a higher in-cylinder pressure and aHRR, thereby resulting in a higher IMEP and ITE. The increase of the IMEP up to 3 bar (~30% improvement) and the increase of ITE is ~10% when increasing the H_2 content from 0% to 60%, which is independent of the charge-air temperature.
(4) The addition of the H_2 may lead to abnormal combustion such as PREMIER combustion and knocking when H_2 concentration exceeding a specific level ($M_{H2} \geq 40\%$) depending on the charge-air temperature. The PREMIER combustion improves the combustion stability and combustion efficiency. However, heavy knocking lowers the combustion stability and thermal efficiency.
(5) the addition of the H_2 improves the combustion stability based on STFT analysis, which shows a higher pressure oscillation frequency but lower pressure oscillation intensity. However, the appearance of the knocking (e.g., $M_{H2} \geq 40\%$ depending on T_{air}) dramatically reduces the combustion stability, which exhibits a larger pressure oscillation frequency and intensity simultaneously.
(6) the addition of the H_2 reduces cycle-to-cycle variations when $M_{H2} < 20\%$ based on CWT analysis. However, when $M_{H2} \geq 20\%$, no significant effect can be observed with a further increase of M_{H2}. Increasing the charge-air temperature may lead to high CCV due to the appearance of knocking.

Overall, there are many benefits from enriching CH_4 with H_2, for instance, the extension of the flammability limits of the mixtures, enhancing the ignition and combustion stability, improvement of the thermal efficiency and potential reduction of the CO_2, UHC and CO emissions. However, it is worth noting that the increase of M_{H2} enhances the knocking tendency. As such, the higher M_{H2} in the H_2–CH_4 mixture at cold conditions is more beneficial for TF combustion.

Declaration of competing interest

The authors declare that they have no known competing financial interests or personal relationships that could have appeared to influence the work reported in this paper.

Acknowledgments

The present study has been financially supported by the Academy of Finland (Grant Nos. 297248 and 318024) and Fortum-Neste Foundation (grant no. 2020050), which are gratefully acknowledged. The second author has also been financially supported by the Henry-Ford foundation under grant no. 202000063. The authors are thankful to Ranta Olli and Blomstedt Otto for their supports on the engine preparations.

REFERENCES

[1] European Commission. CO2 emission performance standards for cars and vans (2020 onwards). 2021. https://ec.europa.eu/clima/policies/transport/vehicles/regulation_en.

[2] European Environment Agency. Annual mean NO2 concentrations observed at traffic stations. 17 December, 2019. https://www.eea.europa.eu/data-and-maps/figures/annual-mean-no2-concentration-observed-12.

[3] Reitz RD, Ogawa H, Payri R, et al. IJER editorial: the future of the internal combustion engine. Int J Eng Res 2019:1–8.

[4] WKM. The future of the combustion engine/assessment of the diesel engine situation (Wissenschaftliche Gesellschaft fü r Kraftfahrzeug- und Motorentechnik e.V. (WKM)). 2017. https://www.wkm-ev.de/images/20170708-englisch-Die-Zukunft-des Verbrennungsmotors.pdf (accessed 7/2019).

[5] a. USCAR. Summary report on the transportation combustion engine efficiency colloquium held at USCAR. 2010. https://inspire.ornl.gov/Original Document/6c560576-42e1-4d28-a8f7-3b0e151a463e (accessed 7/2019).
b. Swain M, Yusuf M, Dülger Z, Swain M. The effects of hydrogen addition on natural gas engine operation. SAE Technical Paper 1993;932775. https://doi.org/10.4271/932775.

[6] Mehra Roopesh Kumar, Duan Hao, Juknelevičius Romualdas, Ma Fanhua, Li Junyin. Progress in hydrogen enriched compressed natural gas (HCNG) internal combustion engines - a comprehensive review. Renew Sustain Energy Rev 2017;80:1458–98.

[7] Salvi BL, Subramanian KA. Sustainable development of road transportation sector using hydrogen energy system. J Renew Sustain Energy Rev 2015;51:1132–55.

[8] Yu HB, Hu EJ, Cheng Y, Yang K, Zhang XY, Huang ZH. Effects of hydrogen addition on the laminar flame speed and Markstein length of premixed dimethyl ether-air flames. Energy Fuels 2015;29:4567–75.

[9] Karim G. Hydrogen as a spark ignition engine fuel. Int J Hydrogen Energy 2003;28:569–77.

[10] Verhelst S, Wallner T. Hydrogen-fueled internal combustion engines. Prog Energy Combust Sci 2009;35:490–527.

[11] Liu WS, Wang Y, Zheng QZ, et al. Study of the effects of adding hydrogen to diesel/CNG dual fuel engine on the emission and fuel consumption. J Combust Sci Technol 2003;9(6):539–45.

[12] Zhou JH, Cheung CS, Leung CW. Combustion, performance and emissions of a diesel engine with H_2, CH_4 and H_2–CH_4 addition. Int J Hydrogen Energy 2014;39(9):4611–21.

[13] Alrazen HA, Abu Talib AR, Ahmad KA. A two-component CFD studies of the effects of H_2, CNG, and diesel blend on combustion characteristics and emissions of a diesel engine. Int J Hydrogen Energy 2016;41(24):10483–95.

[14] Mansor MRA, Abbood MM, Mohamad TI. The influence of varying hydrogen-methane-diesel mixture ratio on the combustion characteristics and emissions of a direct injection diesel engine. Fuel 2017;190:281–91.

[15] Abu-Jrai AM, Al-Muhtaseb AH, Hasan AO. Combustion, performance, and selective catalytic reduction of NOx for a diesel engine operated with combined tri fuel (H_2, CH_4, and conventional diesel). Energy 2017;119:901–10.

[16] Kyrtatos Panagiotis, Brückner Clemens, Boulouchos Konstantinos. Cycle-to-cycle variations in diesel engines. Appl Eenergy 2016;171:120–32.

[17] Heywood JB. Internal combustion engine fundamentals. New York: McGraw-Hill; 1988.

[18] Pera C, Knop V, Reveillon J. Influence of flow and ignition fluctuations on cycle-to-cycle variations in early flame kernel growth. Proc Combust Inst 2015;35:2897–905.

[19] Zhang HG, Han XJ, Yao BF, Li GX. Study on the effect of engine operation parameters on cyclic combustion variations and correlation coefficient between the pressure-related parameters of a CNG engine. Appl Eenergy 2013;104:992–1002.

[20] Rashidi M. The nature of cycle-by-cycle variation in the SI engine from high speed photographs. Combust Flame 1981;42:111–22.

[21] Bizon K, Continillo G, Lombardi S, Sementa P, Vaglieco BM. Independent component analysis of cycle resolved combustion images from a spark ignition optical engine. Combust Flame 2016;163:258–69.

[22] Curto-Risso PL, Medina A, Calvo Hernández A, Guzmán-Vargas L, Angulo-Brown F. On cycle-to-cycle heat release variations in a simulated spark ignition heat engine. Appl Eenergy 2011;88:1557–67.

[23] Vermorel O, Richard S, Colin O, Angelberger C, Benkenida A, Veynante D. Towards the understanding of cyclic variability in a spark ignited engine using multi-cycle LES. Combust Flame 2009;156:1525–41.

[24] Koch J, Schmitt M, Wright YM, Steurs K, Boulouchos K. LES multi-cycle analysis of the combustion process in a small SI engine. SAE Int J Eng 2014;7:269–85.

[25] Cheng Qiang, Ahmad Zeeshan, Kaario Ossi, Martti Larmi. Cycle-to-cycle variations of dual-fuel combustion in an optically accessible engine. Appl Eenergy 2019;254:113611.

[26] Kawahara Nobuyuki, Tomita Eiji. Visualization of auto-ignition and pressure wave during knocking in a hydrogen spark-ignition engine. Int J Hydrogen Energy 2009;34(Issue 7):3156–63.

[27] Kawahara Nobuyuki, Kim Yungjin, Wadahama Hisashi, Tsuboi Kazuya, Tomita Eiji. Differences between PREMIER combustion in a natural gas spark-ignition engine and knocking with pressure oscillations. Proc Combust Inst 2019;37(Issue 4):4983–91.

[28] Kyrtatos Panagiotis, Zivolic Antonio, Brückner Clemens, Boulouchos Konstantinos. Cycle-to-cycle variations of NO emissions in diesel engines under long ignition delay conditions. Combust Flame 2017;178:82–96.

[29] Xu He, Hou Xinghe, Yang Qing, Ma Xiqun, Tian Guohong, Liu Fushui. Study of laminar combustion characteristics of gasoline surrogate fuel-hydrogen-air premixed flames. Int J Hydrogen Energy 2019;44(Issue 26):13910–22.

[30] Sharma Priybrat, Dhar Atul. Effect of hydrogen fumigation on combustion stability and unregulated emissions in a diesel fuelled compression ignition engine. Appl Eenergy 2019;253:113620.

[31] Wu H-W, Wu Z-Y. Investigation on combustion characteristics and emissions of diesel/hydrogen mixtures by using energy-share method in a diesel engine. Appl Therm Eng 2012;42:154–62.

[32] Talibi M, Hellier P, Morgan R, Lenartowicz Ch, Ladommatos N. Hydrogen-diesel fuel co-combustion strategies in light duty and heavy duty CI engines. Int J Hydrogen Energy 2018;43:9046–58.

[33] Tsujimura T, Suzuki Y. The utilization of hydrogen in hydrogen/diesel dual fuel engine. Int J Hydrogen Energy 2017;42:14019–29.

[34] Allenby S, Chang W-C, Megaritis A, Wyszyński ML. Hydrogen enrichment: a way to maintain combustion stability in a

natural gas fuelled engine with exhaust gas recirculation, the potential of fuel reforming. Proc Inst Mech Eng - Part D J Automob Eng 2001;215(3):405–18.
[35] Wing RD. The rotary fuel-injection pump as a source of cyclic variation in diesel engines, and its effect on nitric oxide emissions. Proc Inst Mech Eng 1975;189:497–505.
[36] Stankovic L, Bohme JF. Time-frequency analysis of multiple resonances in combustion engine signals. Signal Process 1999;79:15–28.
[37] Payri F, Broatch A, Tormos B, Marant V. New methodology for in-cylinder pressure analysis in direct injection diesel engines - application to combustion noise. Meas Sci Technol 2005;16(2):540–7.
[38] Kumar P, Foufoula-Georgiou E. Wavelet analysis for geophysical applications. Rev Geophys 1997;35:385–412.
[39] Sen Asok K, Zheng Jianjun, Huang Zuohua. Dynamics of cycle-to-cycle variations in a natural gas direct-injection spark-ignition engine. Appl Eenergy 2011;88(Issue 7):2324–34.
[40] Sen AK, Litak G, Yao B-F, Li G-X. Analysis of pressure fluctuations in a natural gas engine under lean burn conditions. Appl Therm Eng 2010;30(Issues 6–7):776–9.
[41] Sen AK, Litak G, Taccani R, Radu R. Wavelet analysis of cycle-to-cycle pressure variations in an internal combustion engine, Chaos. Solitons Fract 2008;38:886–93.
[42] Sen AK, Longwic R, Litak G, Gorski K. Analysis of cycle-to-cycle pressure oscillations in a diesel engine. Mech Syst Signal Process 2008;22:362–73.
[43] Sen AK, Litak G, Yao BF, Li GX. Analysis of pressure fluctuations in a natural gas engine under lean burn conditions. Appl Therm Eng 2009;30:776–9.
[44] Sen AK, Litak G, Finney CEA, Daw CS, Wagner RM. Analysis of heat release dynamics in an internal combustion engine using multifractals and wavelets. Appl Energy 2010;87:1736–43.
[45] Payri R, Salvador FJ, Gimeno J, De la Morena J. Influence of injector technology on injection and combustion development – part 1: hydraulic characterization. Appl Energy 2011;88:1068–74.
[46] Raju Pradeep, Masimalai Senthil Kumar, Ganesan Nataraj, Karthic SV. Engine's behavior on hydrogen addition of waste cooking oil fueled light duty diesel engine - a dual fuel approach. Energy 2020;194:116844.
[47] Serrano J, Jiménez-Espadafor FJ, López A. Analysis of the effect of different hydrogen/diesel ratios on the performance and emissions of a modified compression ignition engine under dual-fuel mode with water injection. Hydrogen-diesel dual-fuel mode, Energy 2019;172:702–11.
[48] Lee Chia-fon, Pang Yuxin, Wu Han, Hernández Juan J, Zhang Saifei, Liu Fushui. The optical investigation of hydrogen enrichment effects on combustion and soot emission characteristics of CNG/diesel dual-fuel engine. Fuel 2020;280:118639.
[49] Lakshminarayanan PA, Aghav YV. Ignition delay in a diesel engine. In: Modelling diesel combustion. Mechanical engineering series. Dordrecht: Springer; 2010.
[50] Khan Nabeel Ali, Boashash B. Instantaneous frequency estimation of multicomponent nonstationary signals using multiview time-frequency distributions based on the adaptive fractional spectrogram. IEEE Signal Process Lett 2013;20:157–60.
[51] Karimkashi Shervin, Kahila Heikki, Kaario Ossi, Larmi Martti, Vuorinen Ville. Numerical study on tri-fuel combustion: ignition properties of hydrogen-enriched methane-diesel and methanol-diesel mixtures. Int J Hydrogen Energy 2020;45(7):4946–62.
[52] Karimkashi Shervin, Kahila Heikki, Kaario Ossi, Larmi Martti, Vuorinen Ville. A numerical study on combustion mode characterization for locally stratified dual-fuel mixtures. Combust Flame 2020;214:121–35.